# Attraction Force Characteristics Engendered by **Bounded, Radially Diverging Air Flow**

When axially directed air flow enters a parallel plate passage through a hole in one of the plates, the ensuing diverging radial flow is such that a depressed pressure region occurs to some extent over the inlet region of the passage. If the plate against which the inlet air stream impinges is allowed to move freely, it will, under proper flow and other conditions, assume a position of stable equilibrium reflecting a balance among plate weight, the momentum repelling force of the stream, and a net restraining attraction force due to the radial pressure distribution in the passage. This phenomenon, the "Bernoulli" or "axi-radial" effect, has long been of interest in areas such as gas film lubrication and radial diffusers, and it has been applied extensively in IBM systems for contactless transport and motion control of semiconductor wafers on an air film. A steady, laminar, incompressible flow analysis for a representative axisymmetric circular disk model is presented here. A one-dimensional approach, using the general energy equation in conjunction with a passage flow friction factor variation, is applied to obtain an approximate relationship for radial pressure distribution. The friction factor, embodying the influence of varying viscous and inertial forces, is postulated on the basis of specialized radial flow studies in the literature. By also applying the momentum balance condition, an approximate overall solution is obtained which, for arbitrary model dimensions, describes the relationship among equilibrium passage spacing, resultant reaction fluid force and free disk weight, and a flow Reynolds number. The analytical predictions are compared with results from model experiments, and generally favorable agreement is indicated.

# Introduction

The transportation and other motion control of thin, fragile wafers, as required in semiconductor processing, are accomplished under essentially contactless conditions by air film systems developed in IBM [1, 2]. In essence, wafers are moved on a lubricating film of air which exerts prescribed multidirectional control of their motion. The supporting air film combines suction-generating and flowredirection effects based on two fluid mechanics phenomena; thus both attraction and laterally directed control forces are imposed on the wafer. Basically, the film is generated by a symmetric configuration consisting of a flat surface containing an arrangement of recessed, curved-wall regions, or channels. The flat surface portions contain a pattern of small holes of a given internal length through which pressurized air is supplied. Multiple air jets issuing from the holes impinge against the wafer surface and, in turning to flow in essentially radial directions, create local suction regions which collectively act to restrain vertical motion of the wafer. A part of the air flowing radially away from the impact region is redirected down into the curved-wall channels by action of the second phenomenon. This results in a particular augmentation of surface friction effects which, in turn, produce additional control of wafer motion in horizontal directions.

The air film, resulting from the simultaneous action of the above flow effects, characteristically assumes an essentially uniform thickness. A theoretical treatment of the flow behavior in the overall film region, with associated aspects such as variations of film thickness and of forces on the wafer with flow conditions, is extremely complex and is not available. In fact, a comprehensive theoretical

Copyright 1981 by International Business Machines Corporation. Copying is permitted without payment of royalty provided that (1) to republish other excerpts should be obtained from the Editor.

each reproduction is done without alteration and (2) the Journal reference and IBM copyright notice are included on the first page. The title and abstract may be used without further permission in computer-based and other information-service systems. Permission analysis of either of the constituent flow phenomena considered separately also poses formidable difficulties. In relation to the first case, a number of analytical studies have been made, for example, of radial pressure distribution for diverging flow between stationary parallel plates [3-7]. These studies, based on steady, laminar, incompressible flow in a purely radial direction, show the existence of a depressed pressure region associated with the action of both inertial and viscous forces. In the particular situation where a flow jet is introduced through a hole in one of the plates and impinges against the opposite surface, the flow, in turning to the radial direction, separates, in general, to some extent over the lower plate surface. The flow parameters vary in both the transverse and radial directions in the entrance region, and a natural pressure loss occurs here without any actual reduction in the area of the plate passage. An approximate solution describing some of these complex entrance flow characteristics is presented in [8]. It is apparent that an overall theoretical treatment, even for a simple, free-disk, singleinlet-hole, axisymmetric model of this flow phenomenon is quite difficult, since it is keyed to the establishment of an analytical description of the pressure variation over the entire passage. Consequently, the developments described in [1], where this phenomenon and the flow-direction or Coanda effect interact in the air film, were carried out largely by experimental means. In essence, this involved experiments and certain supporting analyses of the first phenomenon treated alone, followed by similar studies of evolved, multiple-jet models of the film surface, where both flow effects are operative.

In this paper, we present an analysis of the suctiongenerating attraction phenomenon, the "Bernoulli" or "axi-radial" effect [1], which is based on a representative, axisymmetric, circular disk model, as shown in Fig. 1(a). Air at density  $\rho$  flows axially through a central tube (radius  $r_i$ , length l) from a reservoir  $s_i$ , where its velocity is practically zero and its pressure is  $p_s$ , and impinges against the upper disk which is free to move in the z direction. From this region, the air stream turns and flows, with no azimuthal variation, radially outward through inlet i of the parallel disk passage (at separation h) to the outlet location o (radius  $r_o$ ). At o the flow emerges into the atmosphere, at which location the pressure is the ambient pressure  $p_a$ . Under proper flow conditions, the free disk of weight W assumes a stable equilibrium position h, in balance with the effects of the momentum repelling force of the air stream and the restraining attraction force due to the net effect of the pressure variation in the flow passage. Characteristically, as the supply flow rate Q is changed, these forces individually assume different values the sum of which is equal to an exerted resultant fluid force S. Thus, for the present case where the disk is allowed to move freely, the reaction to this force is a constant equal to W in accordance with the equilibrium condition. The values of the flow repelling and attraction forces at a given Q are coupled to a particular disk displacement h. Consequently, h varies with Q in a manner that reflects the relative influence of these forces.

The present analysis is based on steady, laminar, incompressible flow conditions. The approximate radial pressure distribution, as influenced by the action of both inertial and viscous forces, is obtained by an axisymmetric, one-dimensional treatment involving the general energy equation in conjunction with a postulated friction factor variation in the flow passage. Using this pressure distribution relationship and accounting for flow energy losses in the inlet tube, an approximate overall solution is obtained by application of the momentum balance condition. The solution describes, for arbitrary model dimensions, the relationship among equilibrium passage spacing, resultant reaction fluid force and free disk weight, and a flow Reynolds number. The analytical predictions are compared with results obtained from experiments with the present model configuration.

The notation used in the following analysis is listed below.

# **Notation**

r,z = radial, transverse coordinates.

h = disk spacing.

 $d_e$  = hydraulic diameter of radial flow passage, 2h.

l = length of axial flow passage.

 $l_d$  = hydrodynamic entrance length of axial passage.

= length ratio,  $l/l_d$ 

p = static pressure (absolute).

 $p_{\star}$  = surrounding atmospheric pressure.

 $\rho = \text{mass density}.$ 

 $\nu$  = kinematic viscosity.

 $\tau_{\rm w}$  = wall shear stress or skin friction.

Q = volumetric flow rate.

u = velocity in the radial direction.

 $U = \text{bulk average velocity}, Q/2\pi rh.$ 

f = friction factor,  $2\tau_{\rm w}/\rho U^2$ .

 $R = \text{local radial passage Reynolds number}, Q/\pi r \nu$ .

 $R_o = R(r/2h)$  = overall Reynolds number,  $Q/2\pi h\nu$ .

 $\bar{r}$  = dimensionless radius,  $2r/h\sqrt{R_o}$ .

 $\bar{z}$  = dimensionless transverse coordinate, 2z/h.

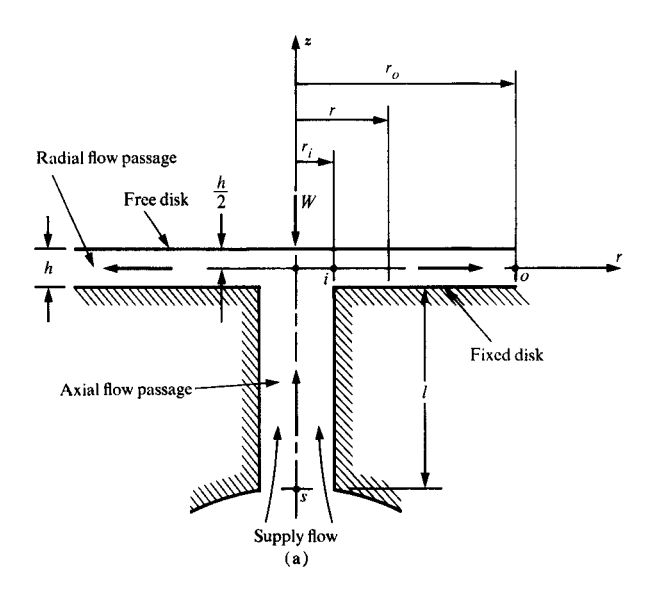
 $\bar{u}$  = dimensionless radial velocity, u/U.

K = constant in the friction factor, Eq. (7).

E = flow energy content at location r.

energy correction factor in pressure distribution,
 Eq. (3).

W =weight of free disk.



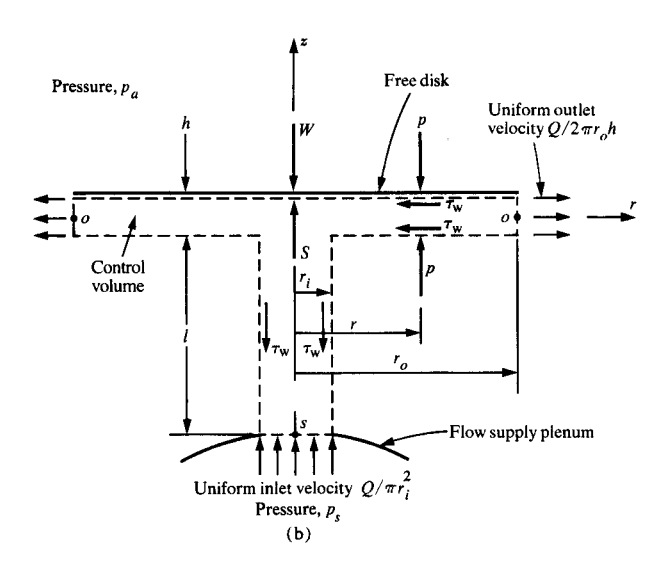


Figure 1 Axi-radial flow model (a) and control volume for the analysis (b).

S = resultant fluid force exerted on disk.

Subscripts: s = supply location.

i = radial passage inlet location.

o = radial passage outlet location.

 $P = \text{dimensionless pressure}, h^2(p - p_a)/4\rho v^2 R_0$ 

F = dimensionless resultant fluid reaction force,  $S/\pi\rho\nu^2$ .

# Analysis

Referring to the model in Fig. 1(a), the free disk of weight W is at an equilibrium displacement h corresponding to a given steady flow rate Q of constant density  $\rho$ , and supplied at a reservoir pressure  $p_s$ . The forces acting on the disk and the conditions for equilibrium are obtained by

application of the momentum principle in conjunction with the control volume in Fig. 1(b). In accordance with the one-dimensional assumptions, the steady flow at the tube inlet (s) and exit (o) regions is taken to be of uniform velocities  $Q/\pi r_i^2$  and  $Q/2\pi r_i h$ , respectively. In addition, the pressure p in the radial passage  $r_i \le r \le r_a$  is taken to be uniform in the z direction and thus varies only with r. Consequently, the pressure (p) and skin friction  $(\tau_w)$  variations with r are the same along both disk surfaces; therefore, it is assumed that a net force that would be exerted on the free disk due to an actual difference in these variations is not existent here. This assumption is considered to be plausible over much of the disk space since  $r_i$  is generally much less than  $r_o$ . In the radial inlet region where the flow parameters vary in both r and z directions, this assumption does not apply to any reasonable extent. Here, the average pressure with respect to the z direction decreases very rapidly to a low value as the flow turns to the radial direction. However, since this decrease, as well as the general two-dimensional flow variations, actually occurs over a small region relative to that of the entire disk space, the basic assumption that p varies only with rfor  $r_i \le r \le r_o$ , where  $r_i << r_o$ , is considered to be a reasonable approximation of the actual overall conditions.

The fluid repelling force for the disk region  $0 \le r \le r$ , is obtained by application of the momentum integral equation [9] with the above assumptions to the control volume of Fig. 1(b). Taking the upward direction as positive, this force is given by  $2\pi \int_0^{r_i} (p - p_a) r dr$  which, in accordance with the momentum balance condition in the z direction, is equal to  $Q^2 \rho / \pi r_i^2 + (p_s - p_a) \pi r_i^2 - 2\pi r_i l \tau_w$ , where  $\tau_w$  is the average skin friction in the inlet tube. The term  $2\pi r_i l \tau_w$ , representing the average flow friction force, is written equivalently as  $\pi r_i^2 \Delta p_s$ , where  $\Delta p_s$  denotes the pressure loss in the tube. In addition to the momentum force, a second force acts on the free disk due to the pressure variation over the surface region  $r_i \le r \le r_o$ . This force is given by  $2\pi \int_{r}^{r_0} (p - p_a) r dr$ . Thus, the resultant fluid force S acting on the disk is equal to the sum of these forces and is

$$S = \pi r_i^2 (p_s - p_a) + \frac{Q^2 \rho}{\pi r_i^2} - \pi r_i^2 \Delta p_s + 2\pi \int_{r_i}^{r_o} (p - p_a) r dr,$$
 (1)

where S may act in the positive or negative directions depending on the relative magnitude of the constituent forces. When the disk is in equilibrium, the weight W acting in the negative downward direction is just equal to S; therefore, the free disk equilibrium condition is given by

$$\pi r_i^2 (p_s - p_a) + \frac{Q^2 \rho}{\pi r_i^2} - \pi r_i^2 \Delta p_s$$

$$-W + 2\pi \int_{r_i}^{r_o} (p - p_a) r dr = 0.$$
 (2)

The pressure distribution relationship p = p(r) for the integration required above is obtained in approximate form by the approach described below.

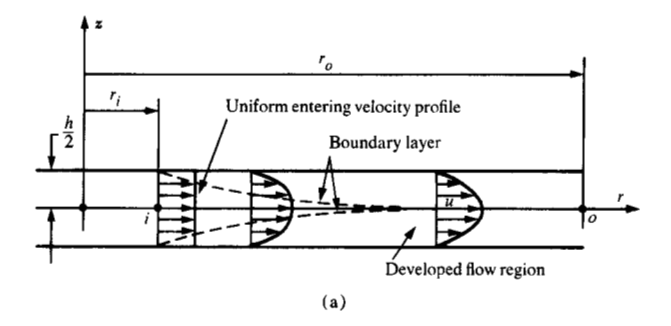
# • Pressure distribution on free disk

In general, the pressure distribution in the overall flow passage reflects the actions of both acceleration and viscous forces even at very low local Reynolds numbers. The acceleration forces are most pronounced in the inlet region of the disk passage, where significant momentum effects are coupled with the flow turning abruptly from the axial to the radial direction. As the flow continues radially outward, these forces gradually decrease as the flow condition is approached where viscous forces are dominant. Characteristically, the flow is of a two-dimensional nature in the inlet region, where flow redirection and separation effects occur, and gradually transforms to a one-dimensional, purely radial character with increase in distance r from the inlet. In the latter region, the transverse velocity profile (u) of the flow approaches the characteristic invariant parabolic form, and the pressure varies logarithmically with radius r. In the inlet region, the velocity profile is of a transversely asymmetric form that varies with r, and the pressure changes in accordance with dominant inertial effects. Between these two limits, the velocity profile and pressure variations with radius reflect the influence of interacting viscous and inertial effects.

For the special case of purely radial flow between stationary disks [Fig. 2(a)], the velocity profile in the idealized situation is uniform at the entry location  $r = r_i$  and, as the flow develops with increasing boundary layer growth, it approaches the invariant parabolic form as  $r \to \infty$ . Livesey [4], in treating the infinite disk condition (i.e., approximated by the condition  $h \ll r_o$ ), assumed a parabolic profile at all radii and using an integral method obtained an approximate solution for the pressure distribution in which both viscous and inertial forces are active. Savage [5] and Jackson and Symmons [6] obtained similar type solutions based on power series expansions of the Navier-Stokes equations with a radially dependent velocity profile. In addition, Boyack and Rice [7] obtained an approximate solution using a different form of radially dependent velocity profile in conjunction with a momentum integral analysis. The basic form of the established dimensionless pressure distribution relationship in the radial passage is given by

$$P = 3 \ln \frac{\tilde{r}_o}{\tilde{r}} - C \left( \frac{1}{\tilde{r}^2} - \frac{1}{\tilde{r}_o^2} \right), \tag{3}$$

where the first and second terms on the right-hand side



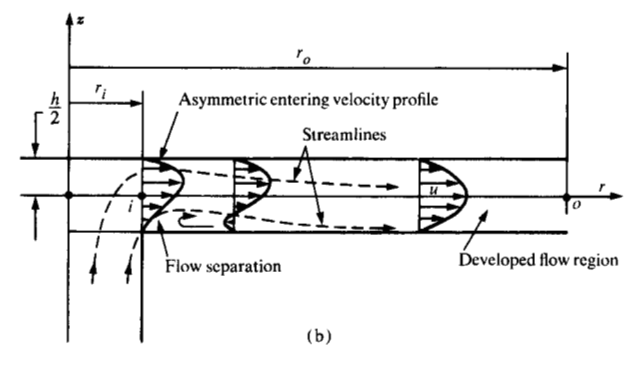


Figure 2 Illustration of purely radial flow characteristics (a) and axi-radial flow characteristics (b).

represent the viscous and inertial pressure effects, respectively. The coefficient C is an energy correction factor, the value of which depends on the shape of the velocity profile. For C = 0.5, the inertia term in Eq. (3) represents the Bernoulli equation. Livesey [4] obtained a value of C = 0.6, which reflects the fact that, for the same average velocity (U), a parabolic velocity profile possesses 20 percent more momentum than a uniform profile. The solutions of Savage [5], Jackson and Symmons [6], and Boyack and Rice [7], all of which are based on a radially varying velocity profile, show values of C = 0.771 (for both [5] and [6]) and C = 0.72, respectively. For  $\bar{r} \rightarrow \bar{r}_i$ (where  $\bar{r}_i \ll \bar{r}_o$ ), the exact pressure distribution solution must approach the Bernoulli equation. Consequently, the above approximations err at small  $\bar{r}$  by at least 20, 54, and 44 percent, respectively.

As  $\tilde{r} \to \tilde{r}_o$ , the inertia term in Eq. (3) becomes much smaller relative to the viscous term, and the dimensionless velocity profile approaches a parabolic form, viz.

$$\bar{u} = \frac{3}{2} (1 - \bar{z}^2). \tag{4}$$

The local friction factor  $f=2\tau_{\rm w}/\rho U^2$ , where  $\tau_{\rm w}=\rho\nu(\partial u/\partial z)_{z=h/2}$  is

$$f = \frac{2\nu}{U^2} \left( \frac{\partial u}{\partial z} \right)_{z=h/2}; \tag{5}$$

thus as  $\bar{r} \rightarrow \bar{r}_o$ , the friction factor approaches the value for fully developed flow, viz.,

$$f \to \frac{24}{R} = \frac{6\bar{r}}{\sqrt{R_0}} , \qquad (6)$$

where R and  $R_o$  are the local and overall Reynolds numbers, respectively. The Livesey solution [4], based on a parabolic profile [Eq. (4)], requires that fR/24 = 1 at all radii, which is physically incorrect since, as  $\tilde{r} \to \tilde{r}_i$ , f must increase due to the increasing influence of the acceleration forces. The radially varying profiles in the other solution methods cited above [5-7] show such an increase in f; however, the results are in considerable disagreement with results from other more valid solutions focusing on the entrance region alone (e.g.), that obtained using the internal boundary layer approximation technique described in [10]). In essence, it is shown that the actual friction factor variation in the flow-developing region is such that as  $\tilde{r} \to \tilde{r}_i$ ,

$$f \to \frac{6K}{\sqrt{R_0}} , \qquad (7)$$

where K is a constant approximately equal to 0.36 for the symmetric entrance configuration of Fig. 2(a). Thus, as  $\bar{r} \to \bar{r}_i$  (where  $\bar{r}_i < K$ ), Eqs. (6) and (7) show that the increasing friction factor in the inlet region can ultimately have a limiting value much greater than that for developed flow.

It is noted that the dimensionless radius  $\bar{r}$  formed from the local radius r, disk spacing h, and the root of the overall Reynolds number  $R_0$  give the local scale of the importance of viscous effects relative to inertial effects, Also,  $R_0$  is not a function of r and, since  $\bar{r}$  is scaled by the  $\sqrt{R_0}$ , small values of  $\bar{r}$  do not necessarily imply small values of physical radii r. Thus, the above limiting friction factor cases, as well as the limiting pressure distribution case [i.e., from Eq. (3)], can be associated with domains not necessarily close to  $r_i$  or  $r_0$ . Finally, the local Reynolds number R, which provides the criterion for the existence of laminar or turbulent flow, is associated with  $R_0$  by the relationship  $R = (2h/r)R_0$ . In the present flow case, h is always much less than local values of r; hence laminar flow values of R correspond to much larger values of  $R_0$ .

In an investigation of radial flow in which viscous and inertial effects interact in a general way, Murphy, Coxon, and McEligot [11] proposed an approximate relationship for the variation of the friction factor in the radial space, as based on a numerical solution of the boundary layer approximations of the Navier-Stokes equations for internal flows. Applying their general results to the configuration of Fig. 2(a), the friction factor variation in the region  $\bar{r}_i \leq \bar{r} \leq \bar{r}_o$  is given by

$$\frac{fR}{24} \approx \sqrt{1 + \left(\frac{K}{\tilde{r}}\right)^2} \quad , \tag{8}$$

where  $K \approx 0.36$ . Thus, for  $\bar{r} \rightarrow \bar{r}_0$  or  $\bar{r} \rightarrow \bar{r}_i$ , Eq. (8) shows that f approaches the limiting cases of Eq. (6) or Eq. (7), respectively. In the intermediate radial region, the f variation is at a maximum deviation of approximately 8 percent from the numerical solution results [11]. In the axiradial configuration of Fig. 2(b), the asymmetric flow in the inlet region is coupled with the existence of separation effects. Hagerup [8], in an investigation of this situation in connection with the inherent restrictor effect in gas bearings, used an integral method to obtain a first approximation to the inlet region energy losses generated by the flow separation behavior. In essence, an examination of these results shows that the limiting inlet region friction factor is actually of the form given by Eq. (7), where K, reflecting the additional influence of the asymmetric condition, now has an apparent average value of approximately 0.4. In a general sense, the flow characteristics of the configurations of Figs. 2(a) and 2(b) are qualitatively similar in that for both cases acceleration effects are dominant in the inlet regions followed by radial transition to developed flow conditions. Consequently, it is assumed that the friction factor variation given by Eq. (8) for the region  $\bar{r}_i \leq \bar{r} \leq \bar{r}_o$ , and with K = 0.4, also represents a good approximation for the axi-radial configuration of Fig. 2(b). Accordingly, this friction factor relationship is used in obtaining the approximate pressure distribution acting on the free disk.

As discussed above, in the region  $r_i \le r \le r_o$ , an average uniform pressure with respect to the z direction is assumed at any radial location in the disk space. The differential energy loss in the radial flow, viz.,  $dE = (2fU^2/d_e)dr$ , becomes upon substitution for  $d_e$ , U, and  $Q = 2\pi h v R_o$ :  $dE = (fv^2 R_o^2/r^2 h) dr$ . Substitution for f from Eq. (8) [with  $R = (2h/r)R_o$  and  $\bar{r} = 2r/h\sqrt{R_o}$ ], integrating between radial locations  $r_o$  and r for fixed values of  $R_o$  and h, and substitution of the results in the general energy equation for steady flow gives the following equation for the pressure distribution:

$$p - p_{a} = \rho \nu^{2} R_{o} \left\{ \frac{12}{h^{2}} \left[ \frac{1}{r} \sqrt{r^{2} + \left(\frac{Kh}{2}\right)^{2}} R_{o} \right] - \frac{1}{r_{o}} \sqrt{r_{o}^{2} + \left(\frac{Kh}{2}\right)^{2}} R_{o} \right\} + \ln \frac{\left( r_{o} + \sqrt{r_{o}^{2} + \left(\frac{Kh}{2}\right)^{2}} R_{o} \right)}{\left( r + \sqrt{r^{2} + \left(\frac{Kh}{2}\right)^{2}} R_{o} \right)} - \frac{R_{o}}{2} \left( \frac{1}{r^{2}} - \frac{1}{r_{o}^{2}} \right) \right] \right\}, \quad (9)$$

or in dimensionless form,

$$P = 3 \left[ \frac{1}{\bar{r}} \sqrt{\bar{r}^2 + K^2} - \frac{1}{\bar{r}_o} \sqrt{\bar{r}_o^2 + K^2} + 1n \frac{(\bar{r}_o + \sqrt{\bar{r}_o^2 + K^2})}{(\bar{r} + \sqrt{\bar{r}^2 + K^2})} \right] - \frac{1}{2} \left( \frac{1}{\bar{r}^2} - \frac{1}{\bar{r}_o^2} \right). \tag{10}$$

By way of comparison, it is seen that, for K = 0, Eq. (10) reduces to Eq. (3) in which C = 0.5. The pressure distribution for the integration required in Eq. (1) or Eq. (2) is thus given by Eq. (9).

# • Free disk equilibrium relationship

For  $\Delta p_s$  in Eq. (1) or Eq. (2), we take into account the additional pressure loss associated with the developing flow condition in the entrance region of the inlet tube [10]. The overall pressure loss that occurs for the ube of length l is written here in the form  $\Delta p_s = \rho U^2$  [8 $l/r_i R_i + 1.14$ ], where  $R_i$  is the local Reynolds number  $Q/\pi r_i \nu$ . In terms of this expression, the tube length required for the fully developed flow condition is given by  $l/r_i = l_d/r_i \ge 0.232 R_i$ . Defining  $l/l_d = k$ , this condition is written as  $l/r_i = k(0.232 R_i)$ , and thus the flow is developed for  $k \ge 1$ . Substituting for  $l/r_i$ , U, and  $R_i$  in terms of  $R_o$  in the above equation for  $\Delta p_s$  gives the following expression for the inlet tube pressure loss:

$$\Delta p_s = \frac{4h^2 \rho \nu^2 R_o^2}{r_i^4} (1.86k + 1.14) . \tag{11}$$

Substitution into Eq. (1) of Eqs. (9) and (11), and for  $p_s - p_a$  obtained by combination of Eq. (9) (with  $r = r_i$ ) and Eq. (11) with the general energy equation, results in the following equation for the resultant fluid force S:

$$\pi \rho \nu^{2} R_{o} \left\{ R_{o} \left[ \frac{4h^{2}}{r_{i}^{2}} \left( 1.86k + 2.14 \right) + \frac{1}{2} \left( \frac{r_{i}^{2}}{r_{o}^{2}} + 1 \right) - \ln \frac{r_{o}}{r_{i}} \right] \right.$$

$$\left. + \frac{12}{h^{2}} \left[ \frac{r_{i}}{2} \sqrt{r_{i}^{2} + \left( \frac{Kh}{2} \right)^{2}} R_{o} \right] \right.$$

$$\left. + r_{o} \left( \frac{1}{2} - \frac{r_{i}^{2}}{r_{o}^{2}} \right) \sqrt{r_{o}^{2} + \left( \frac{Kh}{2} \right)^{2}} R_{o} \right.$$

$$\left. + \left( r_{i}^{2} + \frac{K^{2}h^{2}R_{o}}{4} \right) \ln \frac{\left( r_{o} + \sqrt{r_{o}^{2} + \left( \frac{Kh}{2} \right)^{2}} R_{o} \right)}{\left( r_{i} + \sqrt{r_{i}^{2} + \left( \frac{Kh}{2} \right)^{2}} R_{o} \right)} \right] \right\} = S.$$

$$(12)$$

Substituting  $\bar{r} = 2r/h\sqrt{R_o}$  and  $F = S/\pi\rho\nu^2$ , the dimensionless form of Eq. (12) becomes

$$R_{o} \left[ \frac{34.24}{\tilde{r}_{i}^{2}} (0.87k + 1) \right] + R_{o}^{2} \left[ \frac{3\tilde{r}_{i}}{2} \sqrt{\tilde{r}_{i}^{2} + K^{2}} \right]$$

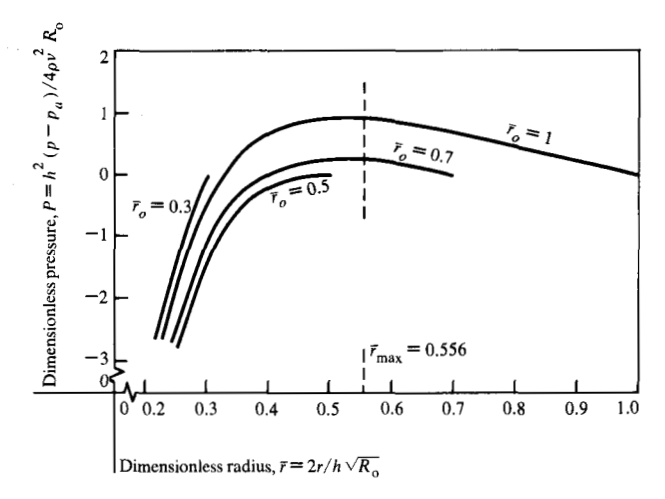


Figure 3 Radial pressure distribution P with dimensionless outer disk radius  $\hat{r}_a$  as parameter [by Eq. (10)].

$$+ 3\bar{r}_{o} \left(\frac{1}{2} - \frac{\bar{r}_{i}^{2}}{\bar{r}_{o}^{2}}\right) \sqrt{\bar{r}_{o}^{2} + K^{2}} + \frac{1}{2} \left(\frac{\bar{r}_{i}^{2}}{\bar{r}_{o}^{2}} + 1\right)$$

$$+ 3 \left(\bar{r}_{i}^{2} + \frac{K^{2}}{2}\right) \ln \frac{(\bar{r}_{o} + \sqrt{\bar{r}_{o}^{2} + K^{2}})}{(\bar{r}_{i} + \sqrt{\bar{r}_{i}^{2} + K^{2}})} - \ln \frac{\bar{r}_{o}}{\bar{r}_{i}}\right] = F.$$
(13)

The free disk equilibrium relationship, Eq. (2), is thus given by Eq. (12) for S = W and in dimensionless form by Eq. (13), where  $F = W/\pi\rho\nu^2$ .

The total pressure drop in the model configuration, viz.,  $p_* - p_a$ , is given by

$$\begin{split} p_{s} - p_{a} &= \rho \nu^{2} R_{o} \bigg[ R_{o} \bigg[ \frac{1}{2r_{o}^{2}} + \frac{4h^{2}}{r_{i}^{4}} \left( 1.86k + 1.14 \right) \bigg] \\ &+ \frac{12}{h^{2}} \bigg[ \frac{1}{r_{i}} \sqrt{r_{i}^{2} + \left( \frac{Kh}{2} \right)^{2} R_{o}} - \frac{1}{r_{o}} \sqrt{r_{o}^{2} + \left( \frac{Kh}{2} \right)^{2} R_{o}} \\ &+ \ln \frac{\left( r_{o} + \sqrt{r_{o}^{2} + \left( \frac{Kh}{2} \right)^{2} R_{o}} \right)}{\left( r_{i} + \sqrt{r_{i}^{2} + \left( \frac{Kh}{2} \right)^{2} R_{o}} \right)} \bigg] \bigg\}. \end{split}$$
 (14)

The dimensionless form of Eq. (14) is

$$P_{s} = \frac{1}{2\tilde{r}_{o}^{2}} + \frac{16}{\tilde{r}_{i}^{4}R_{o}} (1.86k + 114)$$

$$+ 3 \left[ \frac{1}{\tilde{r}_{i}} \sqrt{\tilde{r}_{i}^{2} + K^{2}} - \frac{1}{\tilde{r}_{o}} \sqrt{\tilde{r}_{o}^{2} + K^{2}} \right]$$

$$+ \ln \frac{(\tilde{r}_{o} + \sqrt{\tilde{r}_{o}^{2} + K^{2}})}{(\tilde{r}_{i} + \sqrt{\tilde{r}_{i}^{2} + K^{2}})}, \qquad (15)$$

where 
$$P_{\bullet} = h^2(p_{\bullet} - p_{a})/4\rho v^2 R_{o}$$

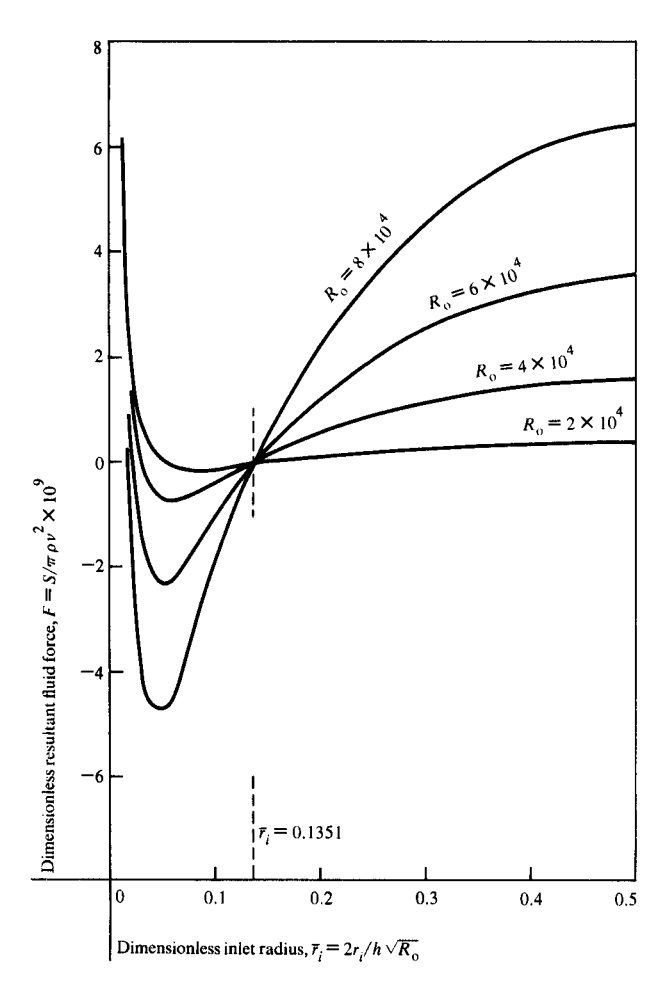


Figure 4 Resultant fluid force F vs  $\tilde{r}_i$ , for  $\tilde{r}_o = 0.5$  and overall Reynolds number  $R_o$  as parameter [by Eq. (13)].

#### Characteristics of the axi-radial flow model

Referring to Eq. (10), the characteristics of the dimensionless pressure distribution P for the case K = 0.4 are illustrated in Fig. 3 for several parametric values of the dimensionless outlet radius  $\bar{r}_a$ . From Eq. (10) it is seen that P has a maximum value at  $\bar{r} = 0.707(-K^2 + \sqrt{K^2 + 0.444})^{1/2}$ = 0.556. Thus, from the definition of  $\bar{r}$  and  $R_0$ , it follows that the physical radius r for maximum P is equal to  $0.556(hQ/8\pi\nu)^{1/2}$ . As seen in Fig. 3, a maximum positive pressure is exhibited only for  $\bar{r}_a$  values greater than 0.556. For  $\bar{r}_a \leq 0.556$ , no maximum exists and the pressures are negative throughout the radial passage. For a value of  $\bar{r}_{a}$  greater than 0.556, it is apparent that a counteracting negative pressure region will occur only for dimensionless inlet radii  $\bar{r} = \bar{r}_i$  less than a particular maximum value. For example, for the cases  $\bar{r}_a = 1$  and  $\bar{r}_a =$ 0.7, the inlet radii  $\tilde{r}_i$  must be less than 0.3 and 0.4, respectively, in order for an attraction force influence to occur.

The characteristics of the dimensionless resultant fluid force F acting on the free disk, as described by Eq. (13)

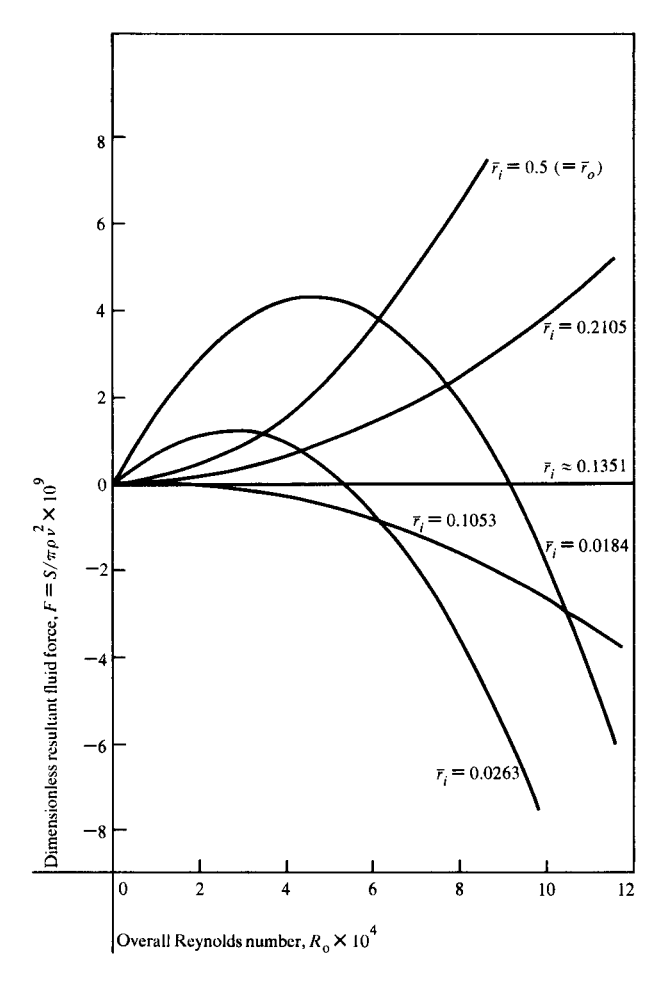


Figure 5 Resultant fluid force F vs  $R_o$ , for  $\tilde{r}_o = 0.5$  and  $\tilde{r}_i$  as parameter [by Eq. (13)].

for values of k = 1 and K = 0.4, are illustrated in Fig. 4 for  $\bar{r}_{o} = 0.5$ . Here, F is plotted against  $\bar{r}_{i}$  with the overall Reynolds number as the parameter. As seen, for the range  $0.1351 \le \tilde{r}_i \le 0.5$ , a repelling resultant force exists, while an attraction resultant force is exhibited for  $\bar{r}_i$  values less than 0.1351. For a given constant value of  $R_0$ , there exists a particular  $\tilde{r}_i$  value for which the attraction force is a maximum; for smaller  $\bar{r}_i$  values, the attraction force decreases as shown. The characteristics of this case are exhibited in a different form in Fig. 5, which shows F plotted against  $R_0$  with  $\bar{r}_i$  as the parameter. As seen, for values of  $\tilde{r}_i < 0.1351$ , the attraction force increases with  $R_0$ . For the particular situation where  $\bar{r}_i$  has a value in the range of 0.1351 to the  $\bar{r}_i$  value where the maximum attraction occurs (Fig. 4), the attraction force decreases continuously over the entire given  $R_0$  range (e.g., as in the case)where  $\bar{r}_i = 0.1053$ ). For  $\bar{r}_i$  values smaller than the low value in this range, a repelling force occurs initially and subsequently decreases with increases in  $R_0$ , e.g., as illustrated by the cases  $\bar{r}_i = 0.0184$  and  $\bar{r}_i = 0.0263$ .

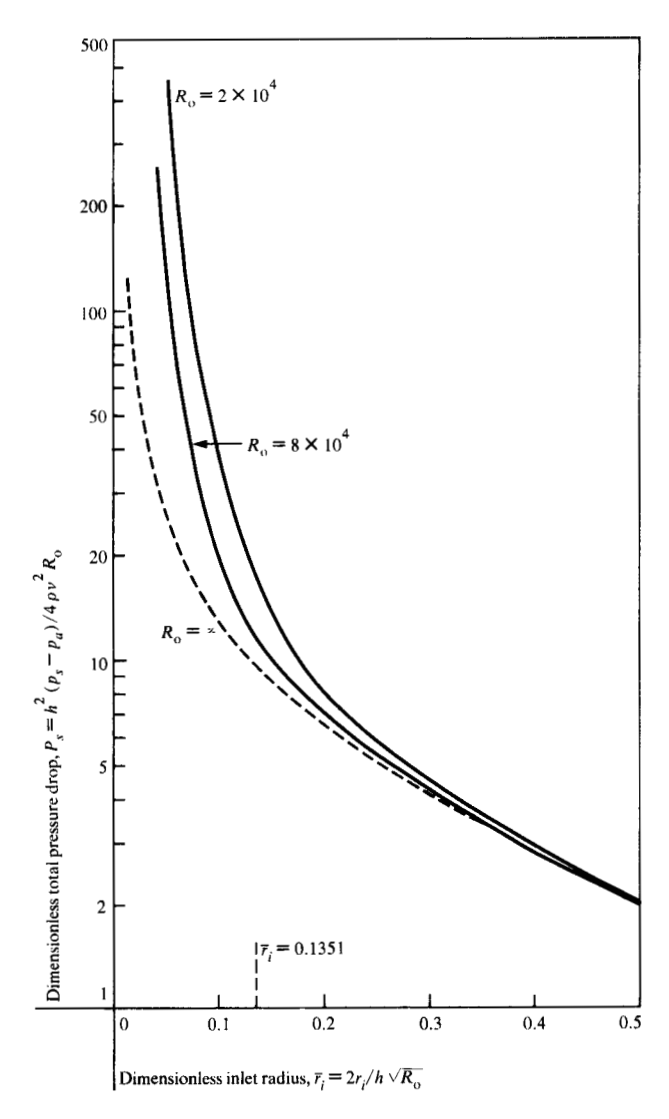


Figure 6 Total pressure drop  $P_i vs \bar{r}_i$ , for  $\bar{r}_o = 0.5$  and overall Reynolds number as parameter [by Eq. (15)].

The variation of the dimensionless total pressure drop  $P_s$  with  $\bar{r}_i$ , as described by Eq. (15) for k=1, K=0.4, and  $\bar{r}_o=0.5$ , is illustrated in Fig. 6 for different values of the parameter  $R_o$ . For values of  $\bar{r}_i>0.1351$ ,  $P_s$  becomes increasingly insensitive to the value of  $R_o$ , while for  $\bar{r}_i<0.1351$  in the disk attraction force range, the sensitivity of  $P_s$  with  $R_o$  is considerable.

# • Experimental verification

A schematic diagram of the basic experimental apparatus that was constructed to study the flow characteristics is shown in Fig. 7. In essence, it consists of a fixed disk and a parallel free disk constrained to accurately controlled motion in the vertical direction by means of a low-friction guide shaft and ball bushing arrangement. The free disk weight is adjusted by means of a lever-arm, sliding-weight

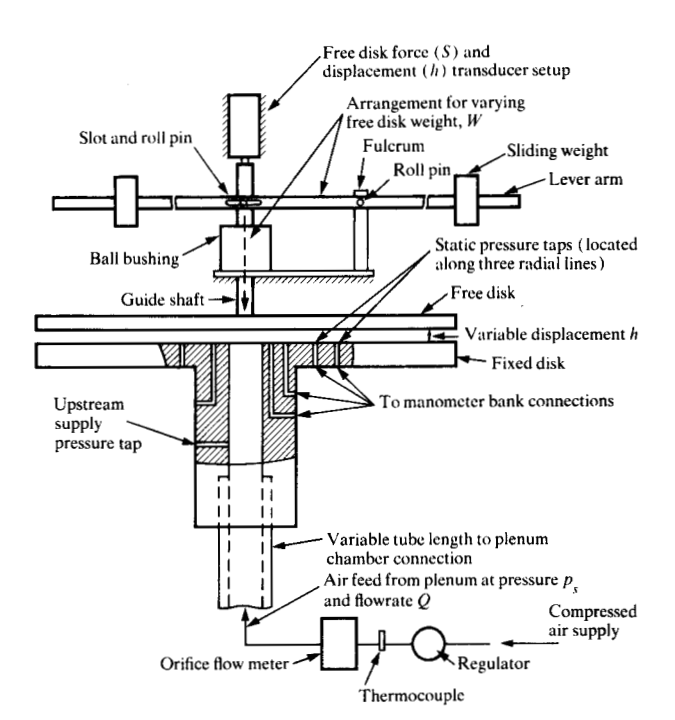
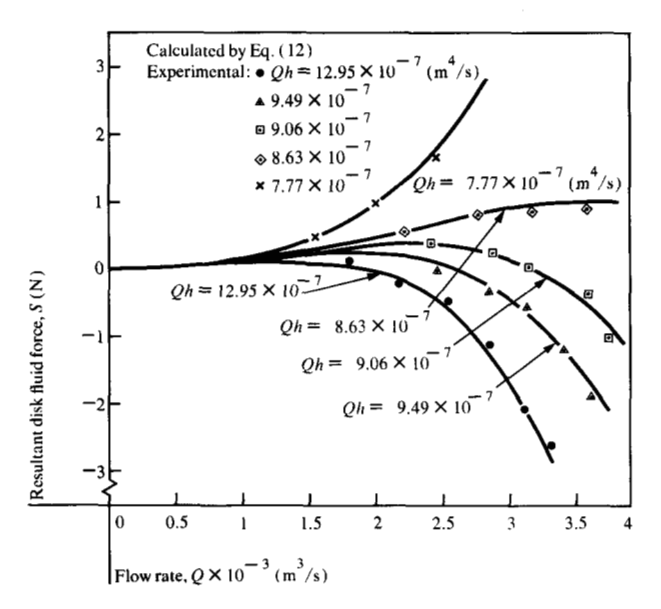


Figure 7 Illustration of the experimental apparatus.

mechanism, which is connected to the guide shaft by a low-friction roll pin arrangement. Thus, a range of free disk weights is obtained by locating the sliding weights at particular distances from the fulcrum. The top part of the guide shaft is attached to a transducer arrangement for measurements of disk displacement and resultant fluid force. The fixed disk is provided with static pressure taps located at different spacing along three radial lines spaced 120 degrees apart. The taps are connected to a manifoldmanometer bank arrangement for measurements of radial pressure distribution. Because of the incorporated axisymmetric flow conditions, the pressure is invariant in the azimuthal direction; hence the static pressure distribution in any given radial direction is provided by all the taps. The fixed disk is connected to a plenum chamber by means of different tube lengths for the purpose of investigating developing inlet flow effects on the overall flow behavior. In operation, metered air is supplied to the disk passage via the plenum at pressure  $p_a$  and flow rate Q. For a given free disk weight adjustment W, measurements are thus made of static pressures p and displacement h. In other experiments, the resultant fluid force S and disk displacement h are measured for various supply flow conditions.

The above experimental technique was used to investigate several combinations of fixed disk inlet and outlet radii for various free disk weight and flow rate conditions. The experimental results reported here were obtained for



**Figure 8** Resultant disk fluid force S vs flow rate Q, with Qh as parameter, for  $r_i = 3.17$  mm and  $r_o = 50.81$  mm; comparison of experiments and calculation by Eq. (12).

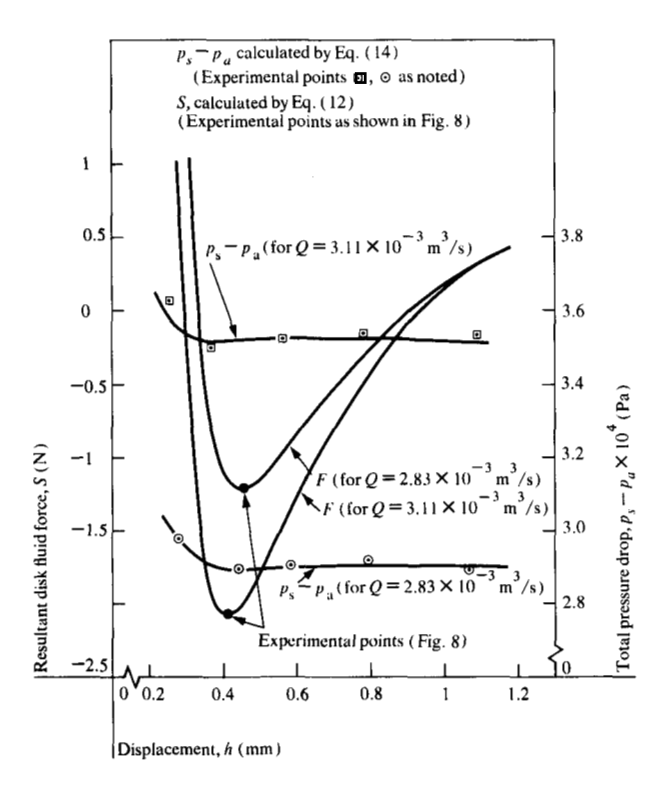


Figure 9 Disk fluid force S and total pressure drop  $p_s - p_a vs$  displacement h, with Q as parameter, for  $r_t = 3.17$  mm and  $r_o = 50.81$  mm; comparison of experiments and calculations by Eqs. (12) and (14).

radii  $r_i = 3.17$  mm and  $r_o = 50.81$  mm, for supply air conditions of  $\rho \approx 1.2$  kg/m<sup>3</sup> and  $\nu = 1.5 \times 10^{-5}$  m<sup>2</sup>/s, and for  $k \approx 1$ . The variation of S with Q for various values of the

parameter Qh, as calculated by Eq. (12), is shown in Fig. 8. As seen, the experimental results also shown on this plot are in very good agreement with the theoretical predictions. Figure 9 shows the corresponding variation of S with h, as illustrated for constant flow rates of  $Q = 2.83 \times$  $10^{-3} \text{ m}^3/\text{s}$  and  $3.11 \times 10^{-3} \text{ m}^3/\text{s}$ . As seen, a maximum attraction force S of approximately -1.2 N occurs at  $h \approx$ 0.45 mm and of -2.05 N at  $h \approx 0.41$  mm for each of these flow rates, respectively. As an illustration of this effect, if the model of Fig. 1 is considered to be in an inverted position, a disk of weight W = 1.2 N will be suspended at  $h \approx$ 0.45 mm for  $Q = 2.83 \times 10^{-3} \text{ m}^3/\text{s}$ , in accordance with the equilibrium condition. From a more general viewpoint, if Q is held constant and h is varied, Fig. 9 illustrates the weight-lifting capability of the overall flow effect, in accordance with the equilibrium condition, S - W = 0. For the model in the upright position shown in Fig. 1, the displacement h and flow rate Q for a disk of a given weight W in equilibrium (viz., S = constant = W) vary as shown in Fig. 8. For example, for a given value of W, Fig. 8 shows the variation of Qh with Q, and thus Q vs h is obtained for the particular disk weight.

For  $Q = 2.83 \times 10^{-3}$  m<sup>3</sup>/s, the overall Reynolds number  $R_0$  is approximately  $6.7 \times 10^4$ . The corresponding local Reynolds numbers R at the inlet and outlet regions are thus 18 900 and 1182, respectively. For  $Q = 3.11 \times$  $10^{-3}$  m<sup>3</sup>/s and  $R_0 \approx 8.1 \times 10^4$ , the local inlet and outlet Reynolds numbers are approximately 20 800 and 1300, respectively. In contrast to the case of flow in a pipe, where  $R \approx 2100$  for the transition from laminar to turbulent flow, no such Reynolds number criterion is available for flows of the present kind. Assuming for the moment that relaminarization occurs for  $R \approx 2100$ , then turbulent flow conditions are indicated from the disk space inlet to  $r \approx 29$  mm and  $r \approx 31$  mm for the first and second flows, respectively. However, in view of the complex situation associated with flow separation and the variable disk space flow area, this assumption is not valid; hence, the actual extent of turbulent flow conditions is not predictable. On the other hand, the favorable agreement indicated between experimental results and the present theoretical treatment is evidently due to the friction factor variation used [i.e., Eq. (8) with  $K \approx 0.4$ ] which approximates the overall effects of these changing flow conditions in the region  $r_i \le r$  $\leq r_o$ . The total pressure drop variation,  $p_s - p_a$ , as calculated by Eq. (14) for each of the above flow rate cases, is also in good agreement with experimental measurements, as shown in Fig. 9. In this particular set of experiments, S was varied, and the flow rate Q was maintained at a constant value by adjusting the pressure  $p_s - p_a$ . As seen,  $p_s - p_a$  initially decreases rapidly with increases in h and eventually assumes an essentially constant value for each of the flow rates.

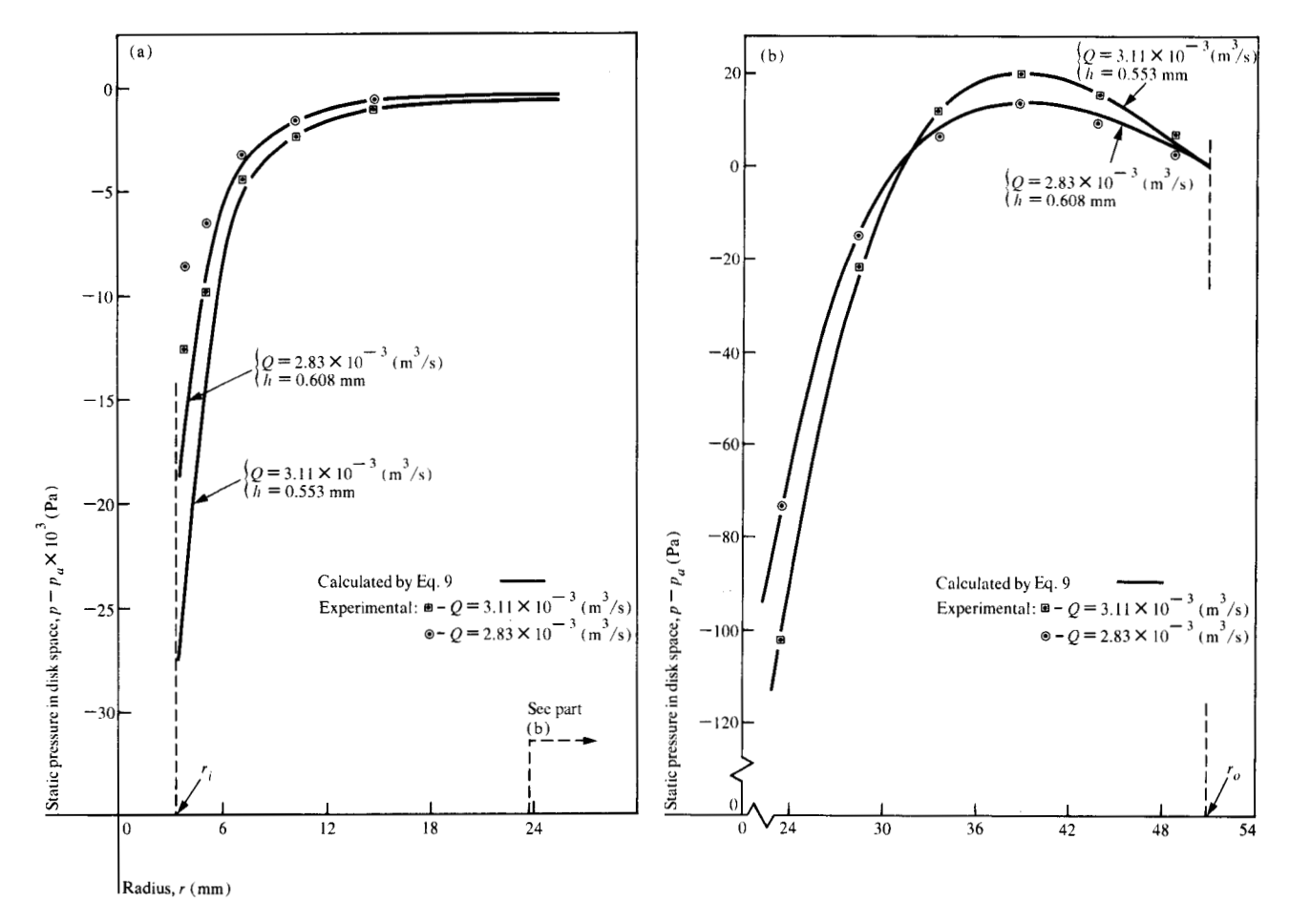


Figure 10 Pressure distribution in disk space  $p - p_a$ , with Q as parameter, for r = 3.17 mm to  $r_a = 23$  mm (a) and for  $r_i = 23$  mm to r = 50.81 mm (b); comparison of experiments and calculations by Eq. (9).

The static pressure distribution in the disk space, as calculated by Eq. (9) for each of the above flow rates, is compared with experimental measurements in Figs. 10(a) and 10(b). The agreement is seen to be good for the radial region beyond  $r \approx 7$  mm. For the immediate inlet region, viz., between  $r_i = 3.17$  mm and  $r \approx 7$  mm, the experimental results differ considerably from the analytical predictions. This is evidently due to the complex flow characteristics in this region, which cannot be accounted for by the present one-dimensional analytical treatment. From an overall viewpoint, however, the present approximate theoretical treatment apparently provides a very good description of the flow characteristics as verified by the favorable agreement with experimental results.

# **Discussion and conclusions**

An approximate analytical description of the overall characteristics of the "axi-radial" flow phenomenon has been obtained on the basis of one-dimensional, steady, laminar, incompressible flow assumptions for a representative

model. The resultant solution, which for arbitrary model dimensions describes the free disk force and displacement relationship with the flow parameters, is keyed to the analytical description of the radial pressure distribution in the flow passage. This description is obtained here by a proposed friction factor variation which reflects the influence of inertial and viscous forces, as well as flow separation effects in the radial inlet region. The occurrence of separation, even for very low Reynolds numbers, induces a highly destabilizing effect to the laminar flow in this region. Thus, the pressure distribution relationship obtained reflects to an extent the effects of the turbulent flow conditions in the upstream region of the passage. The solution, as expressed by Eq. (12), provides a means for determining device dimensions and flow conditions for particular as well as optimal attraction force characteristics. For example, in the particular case considered where  $\bar{r}_a = 0.5$ , it was seen that  $\bar{r}_i$  must be less than 0.1351 in order for an attraction force to develop; also, there exist particular values of  $\bar{r}_i$  and  $R_o$  for which the attraction force is a maximum.

The overall comparison of the present theoretical predictions with experiments is seen to be generally favorable. An exception to this, which apparently does not appreciably influence the other calculated characteristics, concerns the pressure distribution in the inlet region [Fig. 10(a)]. The rapid decrease in pressure from the free disk stagnation value, which occurs as the flow enters the radial region, cannot be described by the present analytical approach. The depressed pressure region described by the analysis predicts lower pressures than those observed experimentally. This disagreement, however, occurs in the immediate vicinity of the inlet region so that its effect on the overall calculated characteristics is apparently small. In experiments with other device dimensions and flow conditions, generally favorable agreement was observed with the analytical predictions. One aspect that was investigated in particular pertained to the developed flow length of the inlet tube [Eq. (11)]. In essence, it was observed that for k < 1 the attraction force diminished and flow instabilities tended to occur. This behavior was most pronounced for k values less than approximately 0.3. For k values greater than approximately 0.8, very stable conditions were observed, which tended to become rapidly insensitive to further increases in k. An analytical description of the latter behavior is also not within the capability of the present one-dimensional model.

The present treatment is based on a single air jet impinging against the free disk. When multiple air jets impinge against the surface, the attraction force is decreased due to flow interaction effects. These effects, in turn, depend on the number of jets as well as their arrangement with respect to a given impingement area. The present solution is not applicable to this case; consequently the wafer air film system developments mentioned earlier [1, 2] were carried out largely by experimental means guided initially by the present analytical results.

## **Acknowledgments**

The assistance provided by C. Davis, Jr., in constructing the various experimental models and apparatus is acknowledged. The very helpful discussion and constructive suggestions offered by F. Hendricks are appreciated.

#### References

- J. A. Paivanas and J. K. Hassan, "Air Film System for Handling Semiconductor Wafers," IBM J. Res. Develop. 23, 361-375 (1979).
- J. A. Paivanas and J. K. Hassan, "A New Air Film Technique for Low Contact Handling of Silicon Wafers," Solid State Technol. 23, 148-155 (1980).
- 3. W. A. Gross, Gas Film Lubrication, John Wiley & Sons, Inc., New York, 1962.
- 4. J. L. Livesey, "Inertia Effects in Viscous Flows," Int. J. Mech. Sci. 1, 84-88 (1959).
- S. G. Savage, "Laminar Radial Flow Between Parallel Plates," ASME J. Appl. Mech. 31, 594-596 (1964).
- J. D. Jackson and G. R. Symmons, "The Pressure Distribution in a Hydrostatic Thrust Bearing," Int. J. Mech. Sci. 7, 239-242 (1965).
- B. E. Boyack and R. E. Rice, "An Integral Solution for the Laminar Radial Outflow of a Viscous Fluid Between Parallel Stationary Disks," ASME J. Basic Eng. 92, 662-663 (1970).
- H. G. Hagerup, "On the Fluid Mechanics of the Inherent Restrictor," ASME J. Fluids Eng. 96, 341-347 (1974).
- G. K. Batchelor, An Introduction to Fluid Dynamics, Second Edition, Cambridge University Press, London, England, 1967, p. 138.
- H. Schlichting, Boundary Layer Theory, Sixth Edition, McGraw-Hill Book Co., Inc., New York, 1968.
- H. D. Murphy, M. Coxon, and D. M. McEligot, "Symmetric Sink Flow Between Parallel Plates," ASME J. Fluids Eng. 100, 477-484 (1978).

Received November 17, 1980; revised December 27, 1980

The authors are located at the IBM General Technology Division laboratory, East Fishkill (Hopewell Junction), New York 12533.